Electronic Supplementary Material (ESI) for Catalysis Science & Technology.

Supporting Information

Confined Co_9S_8 into Defective Carbon Matrix as Bifunctional Oxygen Electrocatalyst for Rechargeable Zinc-Air Battery

Lu Meng,[a] Ling Zhan,[a] Hongliang Jiang,[b] Yihua Zhu,*[a] and Chunzhong Li *[ab]

[a] Key Laboratory for Ultrafine Materials of Ministry of Education, Shanghai Engineering Research Center of Hierarchical Nanomaterials, School of Materials Science and Engineering Institution, East China University of Science and Technology, Shanghai 200237, China.
E-mail: yhuzhu@ecust.edu.cn
[b] School of Chemical Engineering, East China University of Science and Technology, Shanghai 200237, China.
E-mail: czli@ecust.edu.cn.

EXPERIMENTAL SECTION

Regaents. Pt/C (20 wt %) was obtained from Johnson-Mattey. RuO_2 and Nafion solution (5 % wt) were from Sigma-Aldrich. The 2-Methylimidazole (2-MI), zinc nitrate hexahydrate ($Zn(NO_3)_2 \cdot 6H_2O$), cobalt nitrate hexahydrate ($Co(NO_3)_2 \cdot 6H_2O$), potassium chloride (KCl), potassium hydroxide (KOH), methyl alcohol (CH_4O) were obtained from Shanghai Aladdin Bio-Chem Technology Co., LTD. All chemicals were utilized directly as received without any further purification. Ultrapure water was used the whole experiments.

Characterization. Powder X-ray diffraction (XRD) patterns were performed on a Bruker D8. The morphologies and sizes of the sample were observed by using a scanning electron microscopy (FE-SEM: S4800) and transmission electron microscopy (TEM: JEM-2100) at an acceleration voltage of 200 kV. Raman spectroscopy was measured with a laser of 532 nm excitation wavelength. X-ray photoelectron spectroscopy (XPS) measurement was carried out with a VG ESCA 2000 with a magnesium anode for the information of elemental compositions and surface chemical states. The specific surface area and pore size distribution were analyzed by N_2 adsorption-desorption measurement.

Material Synthesis. The synthesis of BMOFs using a modified method and the detailed process were listed in Supporting Information.

Electrochemical Measurements Before using, the working electrode was washed with ultrapure water and alcohol before naturally dried. All electrochemical measurements were performed at room temperature by using a CHI760E (CH Instruments Inc.) and a ring-disk electrode (RRDE,

Pine Instrument) in a three-electrode with a Pt wire and Ag/AgCl (saturated KCl solution) as counter and reference electrodes, respectively. 4 mg catalyst or contrast samples were dispersed in 1 ml mixed solvent (alcohol : Nafion (v/v) = 9 : 1) by sonication to obtain the ink. A 20 μL ink suspension was carefully pipetted onto the glassy carbon electrode surface (5 mm in diameter) and the working electrode was subsequently air-dried at room temperature with a 0.1 mg cm^{-2} catalyst loading on the working electrode. In order to keep the electrolyte saturated with O_2 during the whole measurement, bubbled the O_2 to the solution prior to start measurement for more than 30 min, and maintaining O_2 flow during the whole measurement. The measured potentials were converted to reversible hydrogen electrode (RHE) by the following equation in the paper:

$$E_{RHE} = E_{Ag/AgCl} + 0.0591pH + E^{\theta}_{Ag/AgCl} \quad (1)$$

The Tafel plot is determined by fitting LSV data to the Tafel plot *b*, which is an important parameter to evaluate the activity in the ORR and OER. The Tafel plot was calculated according to Tafel equation:

$$\eta = a + b\,log|J| \quad (2)$$

Where η is the overpotential, *b* is the Tafel plot, and *J* is the current density.

ORR Measurement. The cyclic voltammogram (CV) measurement and the liner sweep voltammogram (LSV) were carried out in an N_2/O_2-saturated 0.1 M KOH solution. The CV tests before and after O_2 purging were recorded at the scan rate of 50 mV s^{-1}. For LSV tests, the scan

rate is 10 mV s^{-1} at varied rotation speeds from 400 to 1600 rpm. The electron transfer number (n) was calculated by the Kouthecky-Levich equation (K-L equation)

$$\frac{1}{J} = \frac{1}{J_L} + \frac{1}{J_K} = \frac{1}{B\omega^{1/2}} + \frac{1}{J_K} \quad (3)$$

$$B = 0.2\, nF\, C_0 (D_0)^{2/3} \nu^{-1/6} \quad (4)$$

where J is the geometric current density, J_L and J_K are the diffusion and kinetic limiting current densities. ω is the rotating speed in 1600 rpm. F is the Faraday constant (96485 C mol^{-1}). C_0 (1.2 $\times 10^{-6}$ mol cm^{-3}) is the bulk concentration of oxygen and D_0 (1.9 $\times$ 10^{-5} cm^2 s^{-1}) is the diffusion coefficient of oxygen. ν (0.01 cm^{-2} s^{-1}) is the viscosity of the electrolyte. The values of C_0, D_0 and ν are all in 0.1 M KOH. For the analysis of peroxide yield, the ring potential was held constant at 1.2 V versus RHE. The percent of H_2O_2 and the number of electron transfer (n) were determined by the following equations

$$\%(H_2O_2) = 200 \cdot \frac{I_r/N}{I_d + I_r/N} \quad (5)$$

$$n = 4 \cdot \frac{I_d}{I_d + I_r/N} \quad (6)$$

where I_d is the disk current, I_r is the ring current, and N (= 0.22) is the current collection efficiency of the Pt ring.

OER Measurements. The catalyst loading and electrolyte for OER performance were the same with the ORR tests, while the OER measurement was carried out at the rotating speed of 1600 rpm in an O_2 saturated 0.1 M KOH solution. The performance was tested at a scan rate of 10 mV s^{-1} with 95 % *iR*-compensation.

Primary Zinc-air Battery Assembly and Testing. Rechargeable Zn-air batteries were constructed in laboratory and tested by CHI 760E. For the air electrode, a carbon paper (7 cm^2) loaded with our own catalyst (7 mg) or commercial Pt/C and RuO_2 catalyst (7 mg, 1/1 molar ratio of Pt/Ru) were used as cathodes, with the catalyst loading of 1 mg cm^{-2}. Meanwhile, the air electrodes also function as the gas diffusion layer and the current collector in assembled batteries. The catalyst was homogeneously sprinkled on air cathode by using an air brush and air-dried for latter using. The electrolyte containing 6 M KOH and 0.2 M zinc acetate full filled the void between two electrodes. Zn foil served as the anode together with a microporous membrane as the separator for the laboratory-constructed Zinc-air battery.

Synthesis the precursor: Typically, the mixture $Zn(NO_3)_2{\cdot}6H_2O$ and $Co(NO_3)_2{\cdot}H_2O$ with desired molar ration of Zn^{2+}/Co^{2+} was dissolved in 40 mL of methanol. A solution of 2-methylimidazole (1.85 g) with 40 ml methanol was added to the above solution with vigorous stirring for 24 h in a constant temperature oven at 30 ºC. The total molar amount of (Zn and Co) was fixed to be 2.825 mmol during the synthesis. The molar ratio of Zn^{2+}/Co^{2+} of the precursor was adjustable over a wide range by varying the initial metallic precursor ratio. The ratios were marked as 20/30/40/50/60, we picked the most remarkable ratio of 40 to carry out the research. The bimetal ZIF was separated by centrifugation and washed thoroughly with methanol for three times, and finally dried overnight at 70 ºC. The precursor power was further grind in quartz mortar.

Synthesis of CE-Co_9S_8@N,S-CM: The bimetallic ZIF precursors were thermally converted into nanoporous carbon through carbonization under flowing argon at 800 ºC for 2 h at the rate of 5 ºC/min. After carefully grinding, the nanoporous carbon was heated with sulfer (5 g) at 800 ºC for 2 h. Thus the nanoporous carbon converted from the bimetal organic framework into N,S co-doped carbon matrix with Co_9S_8.

Synthesis of CE-Co@N-CM: Pick the Zn^{2+}/Co^{2+} of 40, which was testified the best ration in the whole experiment. The dried nanoporous carbon precursor only carbonized at 800 ºC for 2 h at the rate of 5 ºC/min.

Synthesis of Co@N-CM: Pick the Co^{2+}/Zn^{2+} of 0, which the cobalt was the only metal in the precursor. The dried nanoporous carbon precursor only carbonized at 800 ºC for 2 h at the rate of 5 ºC/min.

Synthesis of CoS,Co_9S_8@N,S-CM: Pick the ratio Zn^{2+}/Co^{2+} of 0, which the cobalt was the only metal in the precursor. The grinded ZIF precursors were thermally converted into nanoporous carbon through carbonization under flowing argon at 800 ºC for 2 h at the rate of 5 ºC/min. After carefully grinding, the nanoporous carbon was heated with sulfer (5 g) at 800 ºC for 2 h.

Synthesis of N,S-CM: Pick the ratio Zn^{2+}/Co^{2+} of 1:0, which the zinc was the only metal in the precursor. The grinded ZIF precursors were thermally converted into nanoporous carbon through carbonization under flowing argon at 800 ºC for 2 h at the rate of 5 ºC/min. After carefully grinding, the nanoporous carbon was heated with sulfer (5 g) at 800 ºC for 2 h.

Synthesis of N-CM: Pick the ratio Zn^{2+}/Co^{2+} of 1:0, which the zinc was the only metal in the precursor. The grinded ZIF precursors were thermally converted into nanoporous carbon through carbonization under flowing argon at 800 ºC for 2 h at the rate of 5 ºC/min.

Synthesis of Co_9S_8: 1 mmol of $Co(NO_3)_2.6H_2O$, 2.5 mmol of NH_4F, and 5 mmol of urea were dissolved in 20 mL of deionized water. The solution was transferred into a 40 mL Teflon-lined autoclave and kept at 120 °C for 6 h. After cooling down to room temperature, the pink precursor was washed several times with deionized water. Then, the as-prepared precursor and 0.96 g $Na_2S{\cdot}9H_2O$ were added into 20 mL water under magnetic stirring. The solution was transferred into a 40 mL Teflon-lined autoclave and maintained in an oven at 120 °C for 6 h. Finally, the black Co_9S_8 was collected by filtration, washed with deionized water, and dried overnight at 60 °C under vacuum

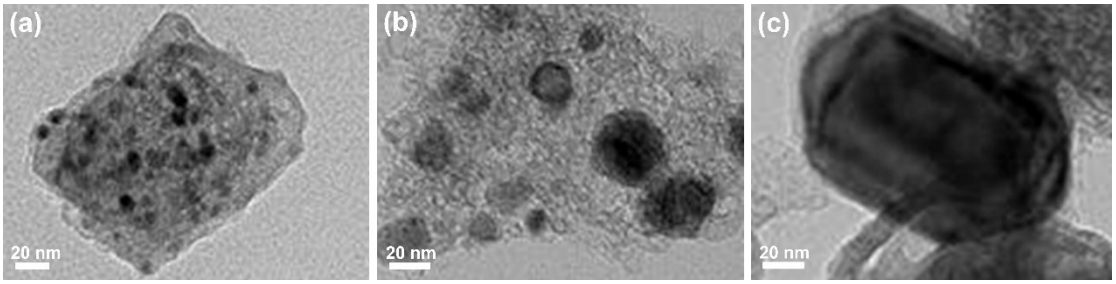

Figure S1. TEM images of (a) CE-Co_9S_8@N,S-CM, (b) CE-Co@N-CM and (c) CoS,Co_9S_8@N,S-CM.

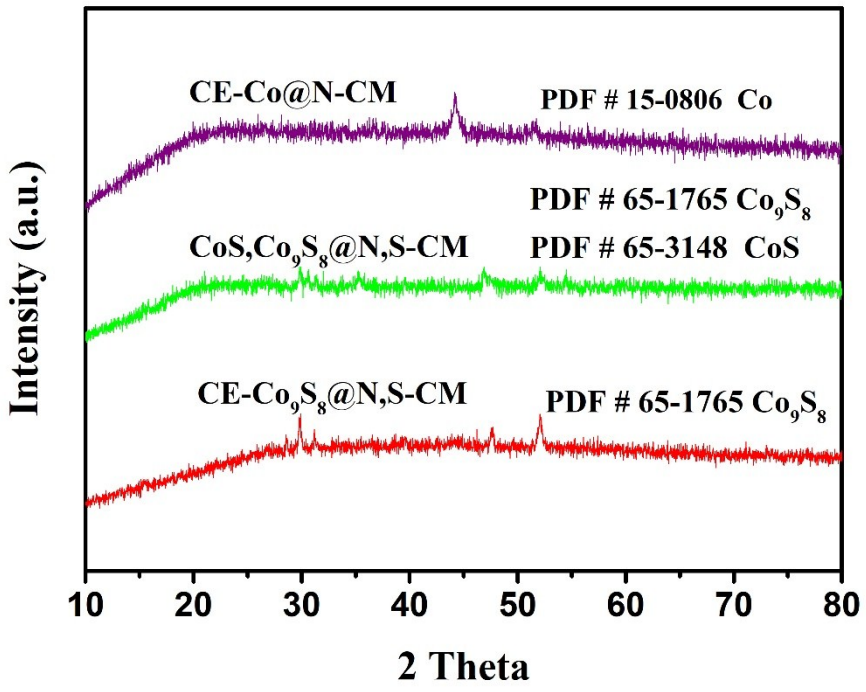

Figure S2. XRD patterns of CE-Co@N-CM, CoS,Co_9S_8@N,S-CM and CE-Co_9S_8@N,S-CM.

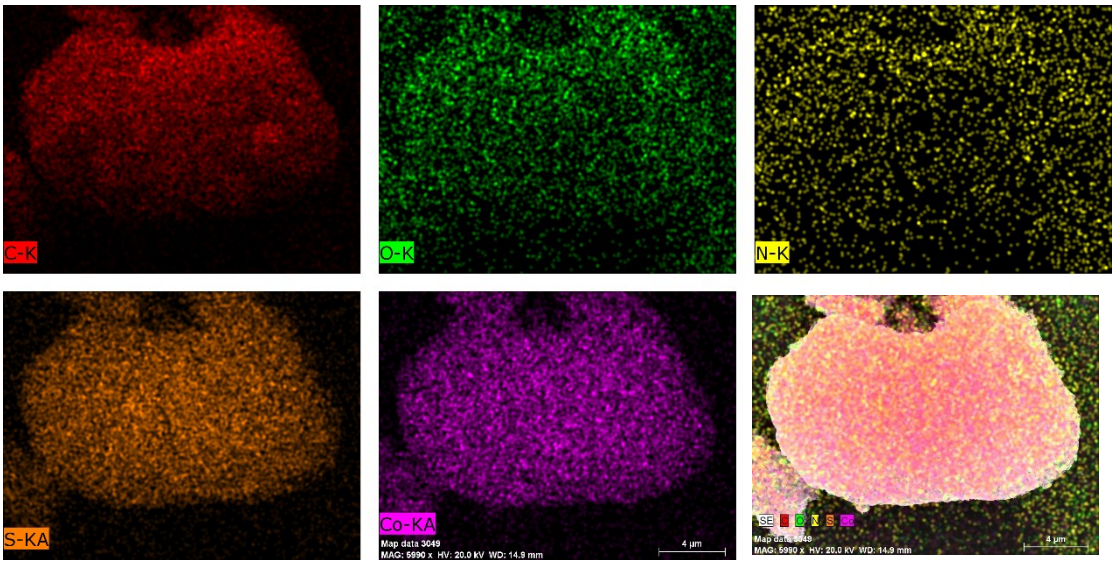

Figure S3. EDX elements mapping images of CE-Co_9S_8@N,S-CM.

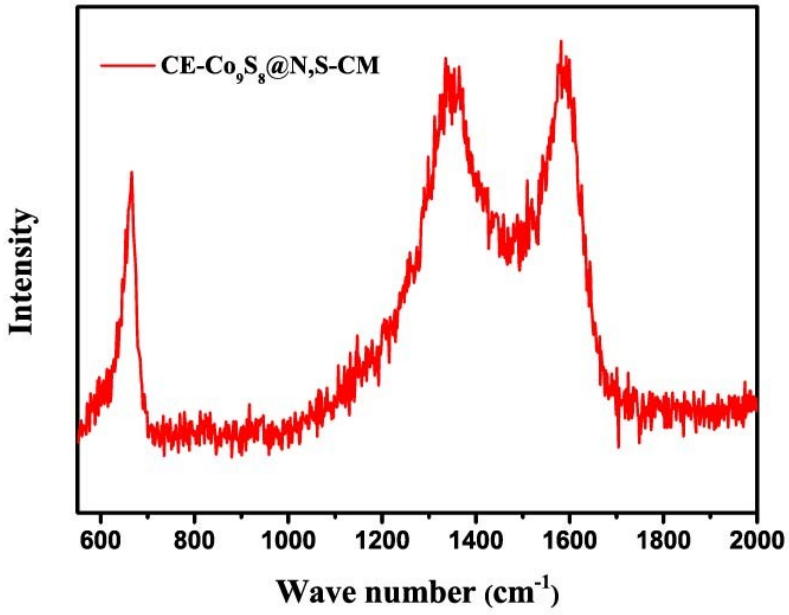

Figure S4. Raman spectrum for CE-Co_9S_8@N,S-CM.

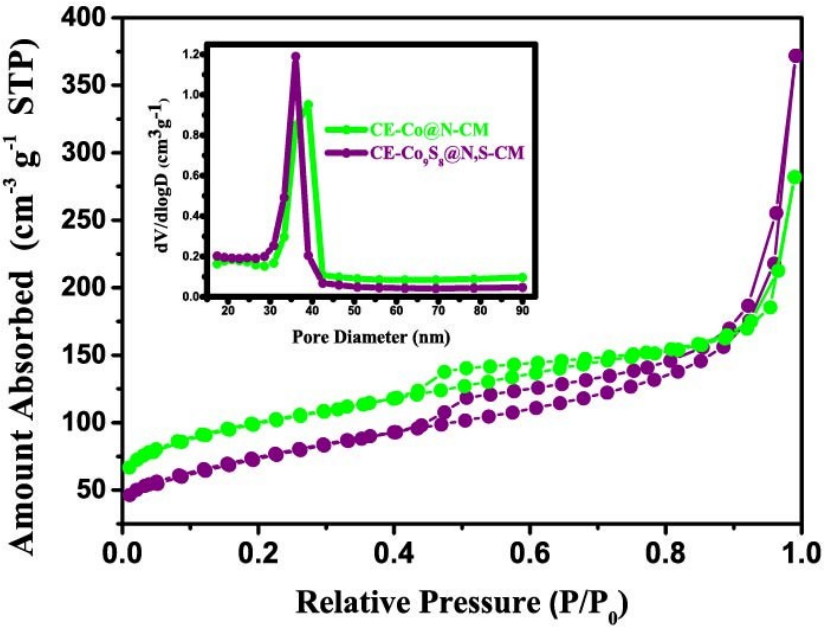

Figure S5. N_2 adsorption/desorption isotherm curves of the CE-Co_9S_8@N,S-CM and CE-Co@N-CM. Inset is the pore size distribution.

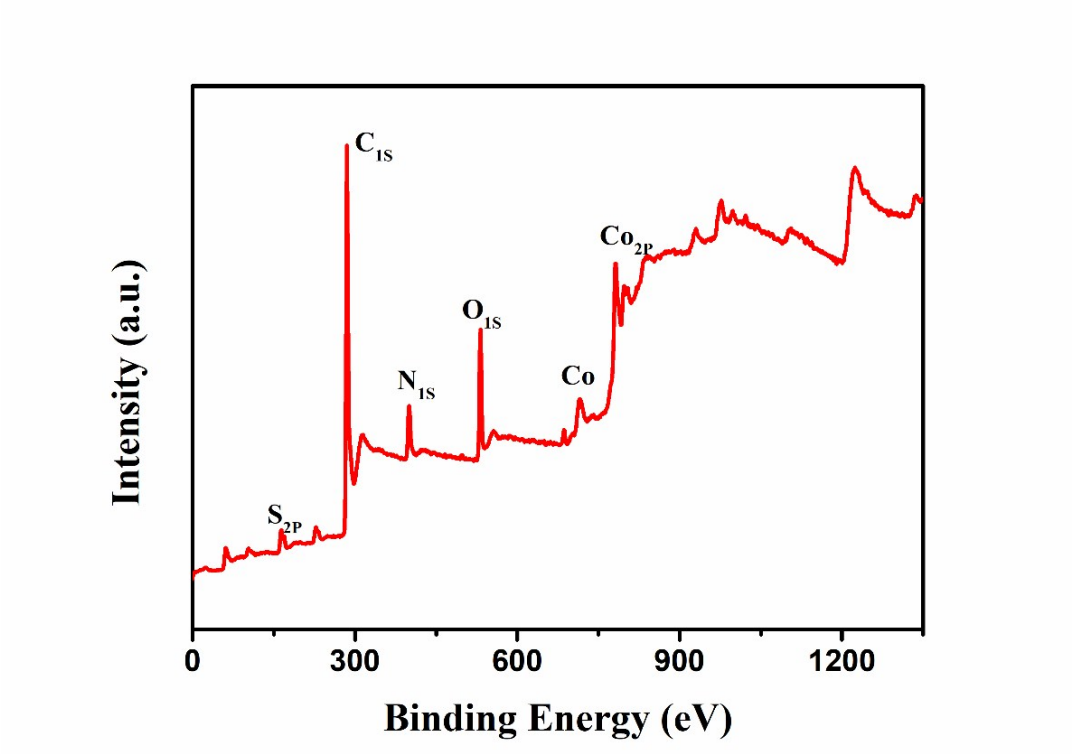

Figure S6. XPS spectrum of CE-Co_9S_8@N,S-CM.

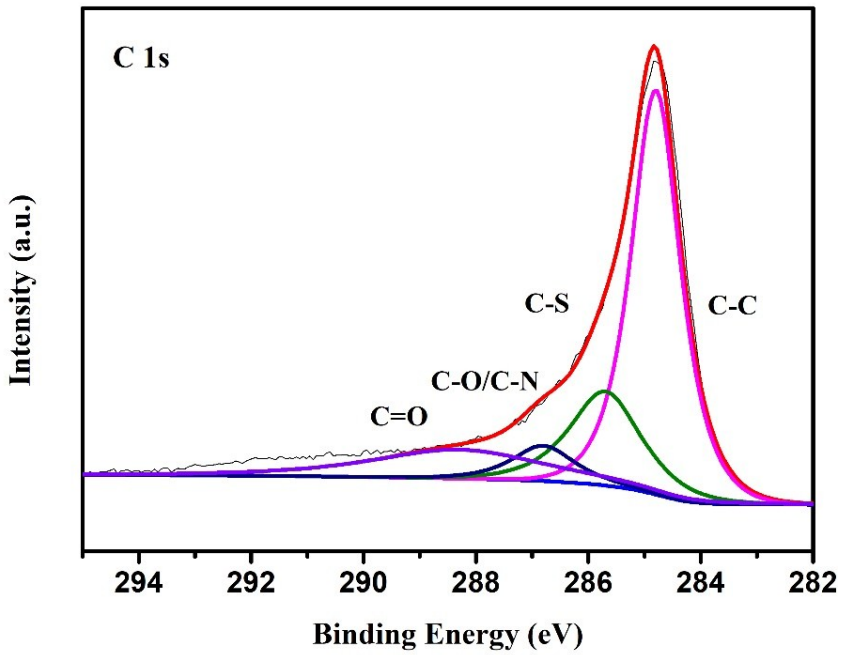

Figure S7. C 1s high-resolution XPS spectrum of CE-Co_9S_8@N,S-CM.

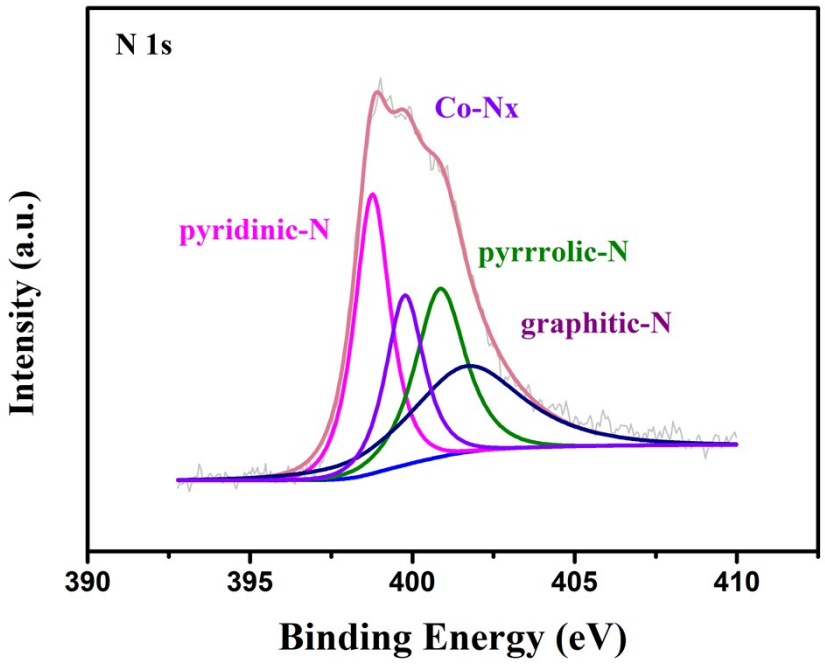

Figure S8. N 1s high-resolution XPS spectrum.

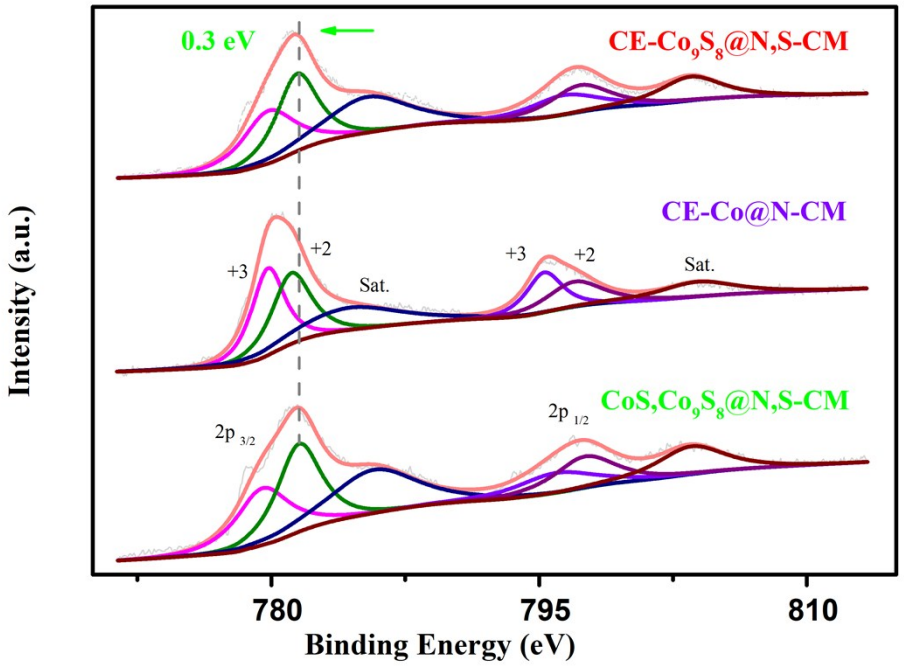

Figure S9. Co 2p high-resolution XPS spectra of CE-Co_9S_8@N,S-CM, CE-Co@N-CM and CoS,Co_9S_8@N,S-CM.

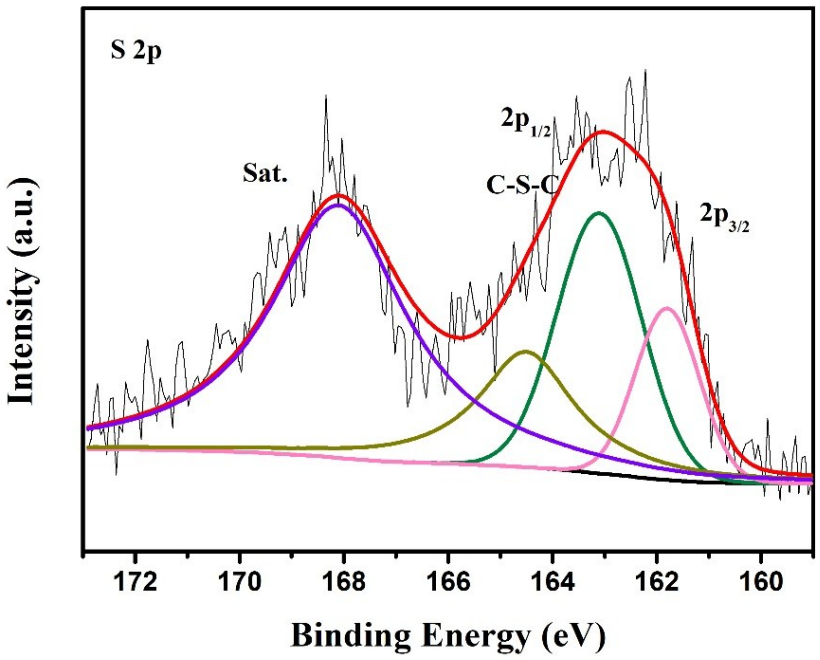

Figure S10. S 2p high-resolution XPS spectrum.

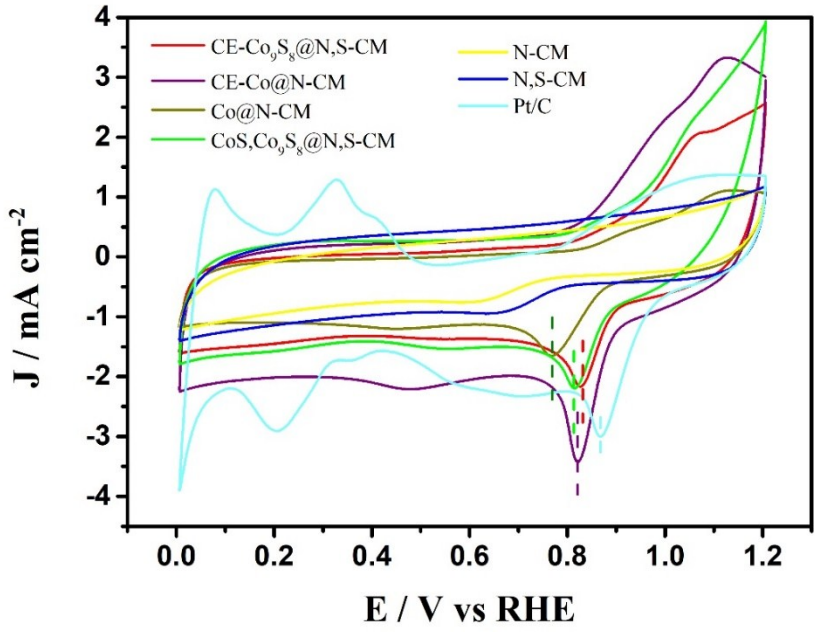

Figure S11. CVs curves of CE-Co_9S_8@N,S-CM, CE-Co@N-CM, CoS,Co_9S_8@N,S-CM, N-CM, N,S-CM and Pt/C at 0.1 M KOH with a scan rate of 50 mV s^{-1}.

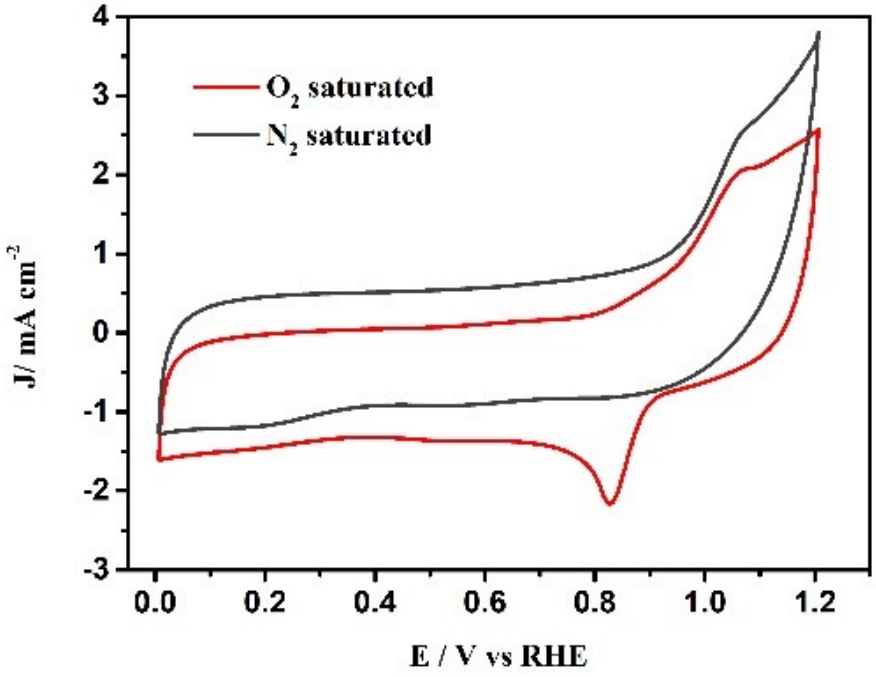

Fig. S12. CVs curves of CE-Co_9S_8@N,S-CM in O_2-saturated and N_2 saturated 0.1 M KOH at a scan rate of 50 mV s^{-1}.

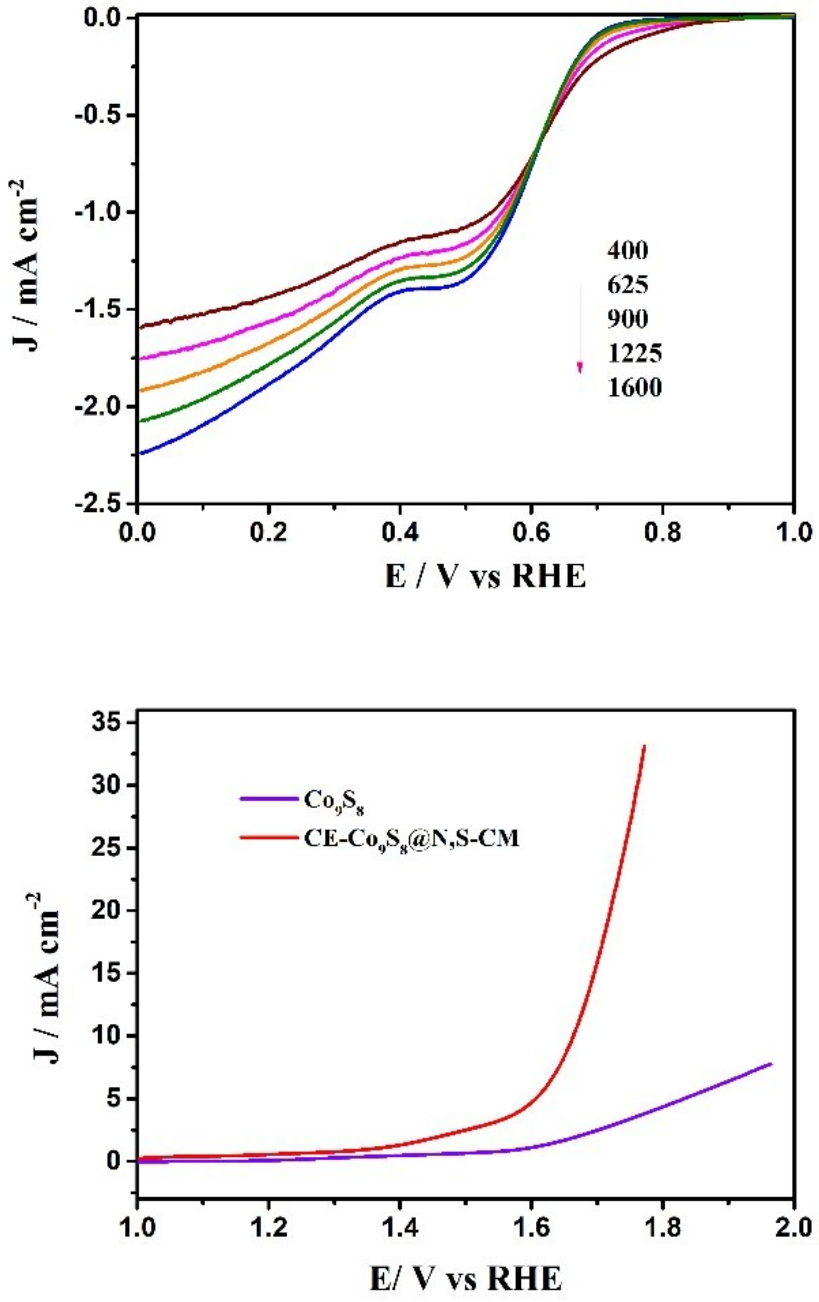

Fig. S 13. Co_9S_8 electrocatalytic in 0.1M KOH (a) ORR polarization curves. (b) OER LSV curves

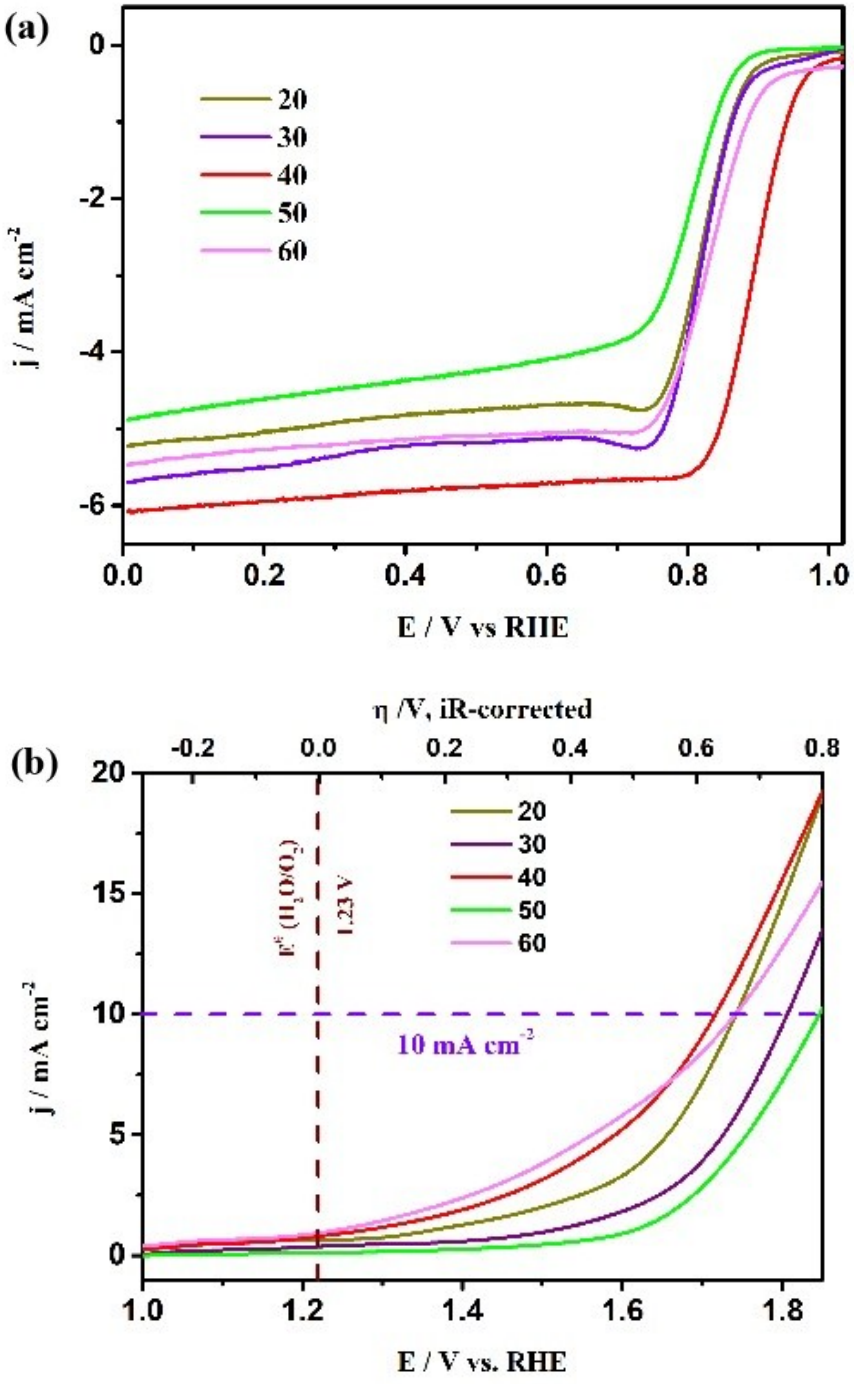

Fig. S14. Different ration of Zn and Co in precursor (a) ORR polarization curves. (b) OER LSV curves.

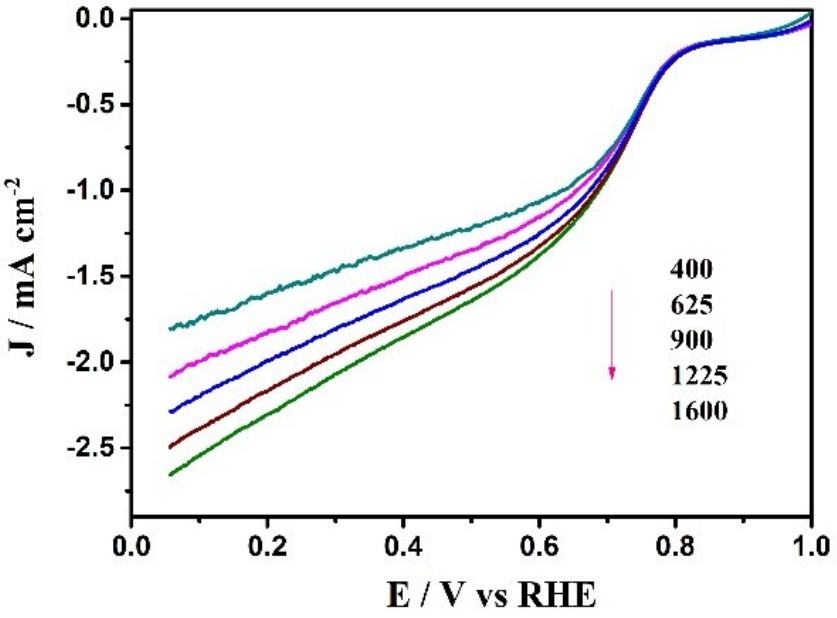

Figure S11 15. CE-Co_9S_8@N,S-CM ORR electrocatalytic in 0.1M $HClO_4$ at different rotation speed.

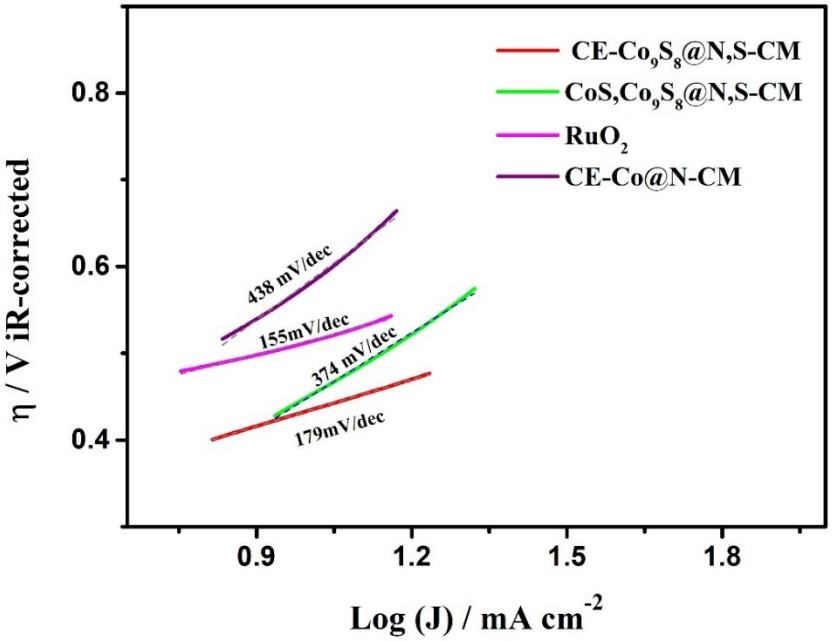

Figure S16. Tafel slopes of CE-Co_9S_8@N,S-CM, CE-Co@N-CM, CoS,Co_9S_8@N,S-CM and RuO_2 electrode

Table S1 The bi-functional electrocatalytic performance comparison between this work and other non-noble metal catalysts.

Sample	Mass loading (mg cm^{-2})	Onset potential (V vs. RHE)	Half-wave potential (V vs. RHE)	Potential Gap ΔE (V)	Ref.
CE-Co_9S_8@N, S-CM	0.40	0.98/	0.88	0.78	This work
Co9S8/NSPG-900	0.283	/	0.80	0.773	1
N-Co_9S_8/G	0.2	0.941	/	0.698	2
(Co_9S_8/N,S-DLCTs)$_{HF}$	0.4	/	0.86	0.70	3
Co_9S_8/N,S-CNTs	1	0.93	0.821	0.78	4
Co_9S_8(800)/N,S-G	0.283	0.931	0.811	0.83	5
Co_9S_8/N, P-APC	0.25	0.89	0.78	0.813	6
Co_9S_8/C	/	0.892	0.778	0.886	7
Co_9S_8@NSC-800	/	0.976	0.865	0.756	8
Co_9S_8/CD@NSC	0.2	/	0.84	0.78	9
Ni3Fe–Co9S8/rGO	0.25	0.91	0.80	0.82	10
Co/S/N‐800	1	0.912	0.831	0.76	11
BNPC-1100	0.4	0.89	0.79	0.89	12

Co/CoO@Co–N-C-800	/	0.91	0.79	0.81	13
NiCo/NLG-270	0.40	0.96	0.82	0.75	14
CoZn-NC-700	0.24	0.98	0.84	0.78	15
Co_9S_8@SNCC	0.40	0.84	0.75	0.81	16
Co_9S_8@NSCM	0.15	0.97	0.81	0.79	17
Co/Co_3O_4@PGS	0.30	0.97	0.89	0.69	18
Co-N@HCS	0.30	0.962	0.864	0.856	19
Co_9S_8/N,S-CNS	0.28	0.90	/	/	20
Co_9S_8/$NSG_{g\text{-}C3N4}$	0.61	0.98	0.86	0.76	21

The compared items including the onset potential (E_{oneset} vs. RHE), half-wave potential ($E_{1/2}$ vs. RHE), and potential gap ($\triangle E$) between the CE-Co_9S_8@N, S-CM with previously reported non-noble metal electrocatalysts.

Supplementary References

1. X. X. Ma, X. H. Dai and X. Q. He, *Acs Sustain Chem Eng*, 2017, **5**, 9848-9857.
2. S. Dou, L. Tao, J. Huo, S. Y. Wang and L. M. Dai, *Energ Environ Sci*, 2016, **9**, 1320-1326.
3. C. C. Hu, J. Liu, J. Wang, W. X. She, J. W. Xiao, J. B. Xi, Z. W. Bai and S. Wang, *Acs Appl Mater Inter*, 2018, **10**, 33124-33134.
4. L. L. Chen, W. X. Yang, X. J. Liu, L. Long, D. D. Li and J. B. Jia, *Nanotechnology*, 2019, **30**.
5. X. X. Ma, Y. Su and X. Q. He, *Chemcatchem*, 2017, **9**, 308-315.
6. X. J. Hu, Y. F. Chen, M. R. Zhang, G. T. Fu, D. M. Sun, O. M. Lee and Y. W. Tang, *Carbon*, 2019, **144**, 557-566.
7. L. H. Li, L. Song, H. Guo, W. Xia, C. Jiang, B. Gao, C. Wu, T. Wang and J. P. He, *Nanoscale*, 2019, **11**, 901-907.
8. S. M. Alshehri, J. Ahmed, A. Khan, M. Naushad and T. Ahamad, *Chemelectrochem*, 2018, **5**, 355-361.
9. P. Zhang, D. Bin, J. S. Wei, X. Q. Niu, X. B. Chen, Y. Y. Xia and H. M. Xiong, *Acs Appl Mater Inter*, 2019, **11**, 14085-14094.
10. X. J. Hu, T. Huang, Y. W. Tang, G. T. Fu and J. M. Lee, *Acs Appl Mater Inter*, 2019, **11**, 4028-4036.
11. N. Jia, J. Liu, Y. S. Gao, P. Chen, X. B. Chen, Z. W. An, X. F. Li and Y. Chen, *Chemsuschem*, 2019, **12**, 3390-3400.
12. Y. H. Qian, Z. G. Hu, X. M. Ge, S. L. Yang, Y. W. Peng, Z. X. Kang, Z. L. Liu, J. Y. Lee and D. Zhao, *Carbon*, 2017, **111**, 641-650.
13. X. Zhang, R. R. Liu, Y. P. Zang, G. Q. Liu, G. Z. Wang, Y. X. Zhang, H. M. Zhang and H. J. Zhao, *Chem Commun*, 2016, **52**, 5946-5949.
14. X. R. Wang, J. Y. Liu, Z. W. Liu, W. C. Wang, J. Luo, X. P. Han, X. W. Du, S. Z. Qiao and J. Yang, *Adv Mater*, 2018, **30**.
15. B. H. Chen, X. B. He, F. X. Yin, H. Wang, D. J. Liu, R. X. Shi, J. N. Chen and H. W. Yin, *Adv Funct Mater*, 2017, **27**.
16. S. W. Liu, M. Y. Tong, G. Q. Liu, X. Zhang, Z. M. Wang, G. Z. Wang, W. P. Cai, H. M. Zhang and H. J. Zhao, *Inorg Chem Front*, 2017, **4**, 491-498.
17. Y. Li, W. Zhou, J. C. Dong, Y. Luo, P. F. An, J. Liu, X. Wu, G. L. Xu, H. B. Zhang and J. Zhang, *Nanoscale*, 2018, **10**, 2649-2657.
18. Y. Jiang, Y. P. Deng, J. Fu, D. U. Lee, R. L. Liang, Z. P. Cano, Y. S. Liu, Z. Y. Bai, S. Hwang, L. Yang, D. Su, W. G. Chu and Z. W. Chen, *Adv Energy Mater*, 2018, **8**.
19. S. C. Cai, Z. H. Meng, H. L. Tang, Y. Wang and P. Tsiakaras, *Appl Catal B-Environ*, 2017, **217**, 477-484.

20. C. Wu, Y. H. Zhang, D. Dong, H. M. Xie and J. H. Li, *Nanoscale*, 2017, **9**, 12432-12440.
21. Y. P. Tang, F. Jing, Z. X. Xu, F. Zhang, Y. Y. Mai and D. Q. Wu, *Acs Appl Mater Inter*, 2017, **9**, 12340-12347.